Available online at www.sciencedirect.com
ScienceDirect
Journal of Nuclear Materials 356 (2006) 280–286
journal of nuclear materials
www.elsevier.com/locate/jnucmat

The NCSU radiation damage database; proton-induced damage energy and application to radiation damage at SINQ

W. Lu [a], M.S. Wechsler [a,*], Y. Dai [b]

[a] Department of Nuclear Engineering, North Carolina State University, Raleigh, NC 27695-7909, USA
[b] Spallation Neutron Source Division, Paul Scherrer Institute, CH-5232 Villigen PSI, Switzerland

Abstract

The NCSU radiation damage database is described. It contains proton and neutron cross sections for production of damage energy, displacements, helium, hydrogen, and heavier transmutation products. The targets in the database include 23 elements from Mg to U and eight practical alloys, but for this paper attention is focused on Al, Fe, and W. Damage energy cross sections are presented for 20–3200-MeV protons based on intranuclear cascade (INC) models (Bertini, CEM2k, and ISABEL) and for 1–2000-MeV protons based on classical Rutherford scattering and SRIM. These cross sections are used to calculate displacement production at SINQ Target 5. It is shown that the SRIM-calculated cross sections can make a significant contribution to proton-induced displacement production in Al at the entrance window and in Fe at Rods 1 and 15.

1. Introduction

Accelerator-driven spallation neutron sources, such as SINQ at the Paul Scherrer Institute (PSI), bombard heavy element targets with high-energy protons. At SINQ the proton energy is 570 MeV, which is sufficiently high so that a number of neutrons per incident proton (about 10) are produced by spallation in its lead target material. Radiation damage is due mainly to the displacement of atoms, but the production of helium, hydrogen, and heavier foreign atoms also plays a part. In spallation neutron sources, these damaging entities are produced by the incident protons and also by the spallation neutrons, which have energies that extend up to that of the incident protons. We refer to the effects of these protons or neutrons as 'spallation radiation damage.' Radiation damage in fission reactor materials has been studied over many years, where the average neutron energy is only about 1–2 MeV and helium production corresponds to less than 1 appm He/dpa. In spallation neutron sources, where the projectile energies extend into the 1 GeV range and hundreds of appm He/dpa may be produced, new techniques are required for the calculation of radiation damage. In particular, cross sections must be calculated for the production of displacements and foreign atoms that apply to the higher neutron and proton energies.

* Corresponding author. Tel.: +1 919 929 5139; fax: +1 919 933 6727.
E-mail address: Wechsler@ncsu.edu (M.S. Wechsler).

0022-3115/$ - see front matter © 2006 Elsevier B.V. All rights reserved.
doi:10.1016/j.jnucmat.2006.05.011

2. NCSU database

A database has been accumulated at NCSU containing damage energy, displacement, helium, hydrogen, and transmutation production cross sections useful for calculating spallation radiation damage. The targets thus far include 23 elements from Mg to U and eight steels and other practical alloys, as follows:

Target elements

Group 1:$_{12}$Mg, $_{13}$Al, $_{14}$Si
Group 2:$_{22}$Ti, $_{23}$V, $_{24}$Cr, $_{25}$Mn, $_{26}$Fe, $_{27}$Co, $_{28}$Ni, $_{29}$Cu
Group 3:$_{40}$Zr, $_{41}$Nb, $_{42}$Mo, $_{47}$Ag, $_{50}$Sn
Group 4:$_{73}$Ta, $_{74}$W, $_{79}$Au, $_{80}$Hg, $_{82}$Pb, $_{83}$Bi
Group 5:$_{92}$U

Target Alloys (compositions used in the calculations given in atomic percent):

AlMg3 (Al–2.72Mg–0.35Mn–0.25Fe)
EP823 (Fe–12Cr–1.8Si–0.9Ni–0.7Mo–0.7Mn)
Eurofer97 (Fe–9Cr–1.1W–0.4Mn)
F82H (Fe–7.9Cr–2.0W–0.2V)
HT9 (Fe–11.8Cr–1.0Mo–0.6Ni–0.5Mn)
SS316L (Fe–17.5Cr–12.2Ni–2.5Mo–1.8Mn)
T91 (Fe–8.6Cr–1.0Mn–0.2Ni)
Zr-2 (Zr–1.36Sn–0.17Fe–0.13O–0.11Cr–0.07Ni)

The alloy compositions include 17 of the 23 target elements.

Proton and neutron projectiles are considered separately in three energy ranges, depending upon applicable codes: (A) $20 < E < 3200$ MeV, (B) $E < 20$ MeV, and (C) $20 < E < 150$ MeV. For Range (A), three intranuclear cascade (INC) models within MCNPX [1] were employed: Bertini, ISABEL, and CEM2k [2]. Also, for Bertini and ISABEL INC models three level-density formulations were used: HETC, GCCI (default), and Jülich with multistage pre-equilibrium on (default) and off. For range (B), we used information from ENDF-6 [3] and SPECTER [4] for neutrons and SRIM [5] for protons. For neutrons in Range (C), the cross sections stem from the LA150 compilations [6].

In this paper, we present damage energy and displacement cross sections for protons, with emphasis on Al, Fe, and W, as representative of light, medium-weight, and heavy target elements.

3. Damage energy and displacement cross sections for protons

By damage energy, we mean the energy delivered to target atoms (perhaps producing atomic displacements), excluding energy delivered to electrons. The partitioning into displacement-producing and electronic components relies on the Lindhard model [7], which permits the calculation of damage energy $\widehat{T}$ as a function of the primary recoil energy T (Eqs. (8) and (9) in ASTM E 521-96 [8]). Then, the damage energy cross section is given by

$$\widehat{\sigma} = \frac{\widehat{T}/n_0}{xN_V}, \tag{1}$$

where n_0 is the number of incident protons, x is the target thickness, and N_V is the number of target atoms per unit volume. For the Bertini and ISABEL INC models we used $n_0 = 10^6$ protons and for CEM2k $n_0 = 10^5$ protons. Also, $x = 0.1$ cm and $N_V = 6.0$, 8.5, and 6.3×10^{22} atoms/cm^3 for Al, Fe, and W, respectively. The displacement cross section is then given by

$$\sigma_d = \frac{\kappa}{2T_d}\widehat{\sigma} = \frac{\kappa}{2T_d}\frac{\widehat{T}/n_0}{xN_V}, \tag{2}$$

where $\kappa = 0.8$ [8] and $T_d = 27$, 40, and 90 eV for Al, Fe, and W, respectively.

Fig. 1 shows damage energy cross section as a function of proton energy in range (A) for Al, Fe, and W, as calculated using the default settings of Bertini, ISABEL, and CEM2k INC models. The cross section for Bertini and ISABEL do not include values below 50 MeV, since 50 MeV is the lower energy limit for the proton elastic scattering model incorporated into LAHET2.8 [9]. Also, the ISABEL model does not calculate cross sections above 1000 MeV. The curves for Al are representative of the three target elements in Group 1, for Fe of the eight elements in Group 2, and for W of the six elements in Group 4. For the INC-based calculations over the range 20–3200 MeV, there is little difference between proton and neutron cross sections (Fig. 2), except near the 20 MeV lower energy limit and for CEM2k values for Fe between at about 500–1200 MeV. It has been known for some time [10,11] that INC-based calculations tend to give significantly lower damage energy and displacement cross sections for neutrons, as compared to values based on ENDF-6, SPECTER (which itself is based on ENDF-5), and LA150. As the origin of the

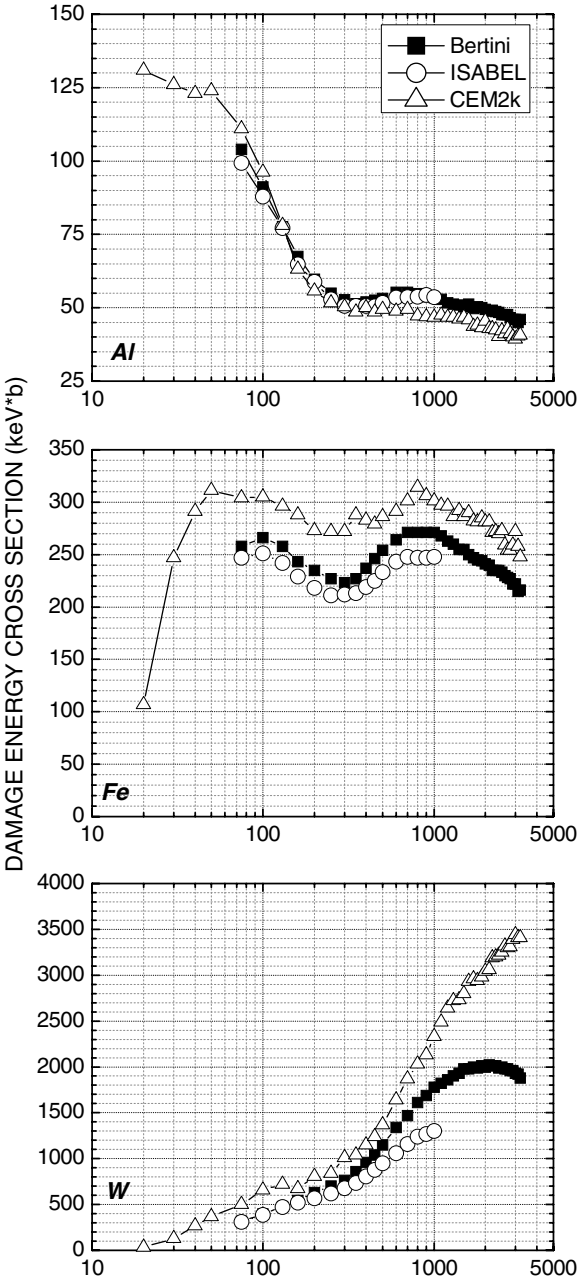

Fig. 1. Damage energy cross section versus proton energy for Al, Fe, and W, as calculated using Bertini, ISABEL, and CEM2k INC models.

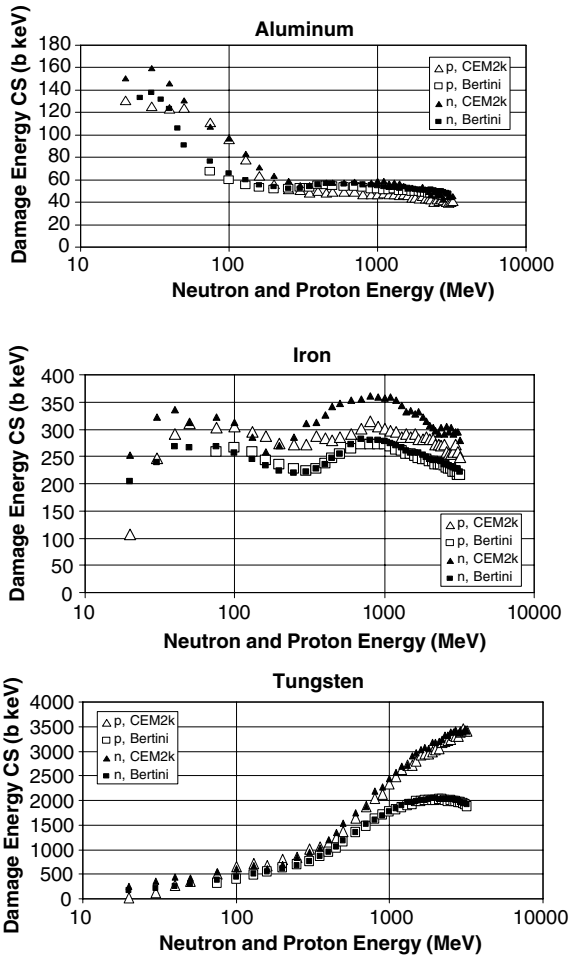

Fig. 2. Damage energy cross section versus incident energy for protons and neutrons on Al, Fe, and W, as calculated using CEM2k and Bertini INC models.

acronym 'ENDF' suggests, it is an evaluated data file in the sense that it considers experimental data in combination with nuclear model calculations in the attempt to determine the true value, and the same is true for LA150. Over a range of targets from Mg to Bi, damage energy cross sections from ENDF-6, SPECTER, and LA150 for 20-MeV neutrons are found to be within 10% of one another. But, the Bertini values for 19 targets from Mg to Pb are low with respect to SPECTER, for example, by an average of 34% [11]. The CEM2k values are within 10% of SPECTER for heavier targets, but for 14 targets from Mg to Mo, CEM2k values are low by an average of 18%. As it agrees better with LA150 and SPECTER, CEM2k is preferred for calculating damage energy or displacement cross sections.

No such body of evaluated damage energy cross sections, as described above, from ENDF and SPECTER for below 20 MeV and LA150 for 20–150 MeV for neutron irradiation is available for proton irradiation. Instead, we have calculated these cross sections using classical Rutherford scattering and SRIM [5]. The differential Rutherford

scattering cross section (differential with respect to transferred recoil energy, T) is given by (Eqn. 4–38 in [12])

$$\sigma'_{\mathrm{T}}(E,T) = \frac{\gamma}{ET^2}, \tag{3}$$

where $\gamma = \pi(Z_1 Z_2 e^2)^2 (M_1/M_2)$, $E =$ incident proton energy, $T =$ energy transferred to the struck target atom (primary knocked-on atom, PKA), Z_1 and Z_2 are the atomic numbers and M_1 and M_2 are the masses of the incident proton and the target atom, respectively, and e is the electron charge. The conventional expression for the displacement cross section, σ_{d}, is

$$\sigma_{\mathrm{d}}(E) = \int_0^{T_{\max}} \sigma_{\mathrm{T}'}(E,T)\nu(T)\mathrm{d}T, \tag{4}$$

where $\nu(T)$ is the multiplication factor, i.e., the number of displacements produced by a PKA of energy T. The current expression for the multiplication factor based on the modified Kinchin–Pease model, as described by Norgett, Robinson, and Torrens [13] and established as a standard by ASTM [8], is

$$\nu(T) = \left\{ \begin{array}{c} 0, T < T_{\mathrm{d}} \\ 1, T_{\mathrm{d}} \leqslant T < \frac{2T_{\mathrm{d}}}{\kappa} \\ \frac{\kappa}{2T_{\mathrm{d}}}\widehat{T}(T), T \geqslant \frac{2T_{\mathrm{d}}}{\kappa} \end{array} \right\} \tag{5}$$

where κ is the displacement efficiency (set equal to 0.8) and $\widehat{T}$ is the damage energy corresponding to T. Substitution of (3) and (5) into (4) gives for the damage energy cross section

$$\widehat{\sigma} = \left(\frac{2T_{\mathrm{d}}}{\kappa}\right)\sigma_{\mathrm{d}} = \left(\frac{\gamma}{E}\right)\left(\frac{2-\kappa}{\kappa} + I\right), \tag{6}$$

where $\kappa = 0.8$ and $I = \int_{2T_{\mathrm{d}}/\kappa}^{T_{\max}} \frac{\xi(T)}{T}\mathrm{d}T$, where $\xi(T) = \widehat{T}/T$. The resulting damage energy cross sections for Al, Fe, and W are shown in Fig. 3, where for the integral I in (6) we used $T_{\mathrm{d}} = 27$, 40, and 90 eV, respectively. In the log–log plot of Fig. 3, the points indicate a slope of -1 due to the $1/E$ dependence in Eq. (3), with a slight additional dependence on E due to the $T_{\max}$ upper limit on the integral I.

Fig. 3 also shows damage energy cross sections obtained using SRIM, which uses a more realistic interatomic potential than the simple expression in Eq. (3), including Coulomb screening, quantum mechanical treatment of ion–atom collisions, and exchange and correlation interactions between overlapping electron shells. Incident energies extend up to 2 GeV/amu. SRIM runs were made for targets

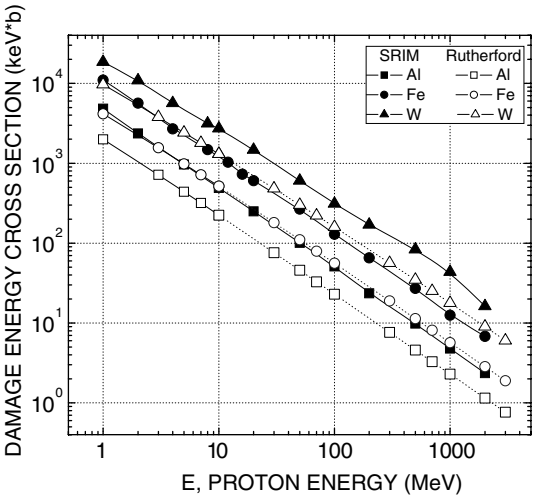

Fig. 3. Damage energy cross sections for protons on Al, Fe and W calculated by SRIM and Rutherford scattering formula.

of varying thickness, and the resulting cross sections were extrapolated to zero thickness, as shown for example for W in Fig. 4. In Fig. 3, the same slope of -1 is seen for SRIM as for Rutherford scattering, but the cross section values from SRIM are a factor of about two higher than those obtained using the Rutherford formula.

The cross sections above 20 MeV from the INC calculations and from the SRIM calculations stem from quite different mechanisms. A reasonable

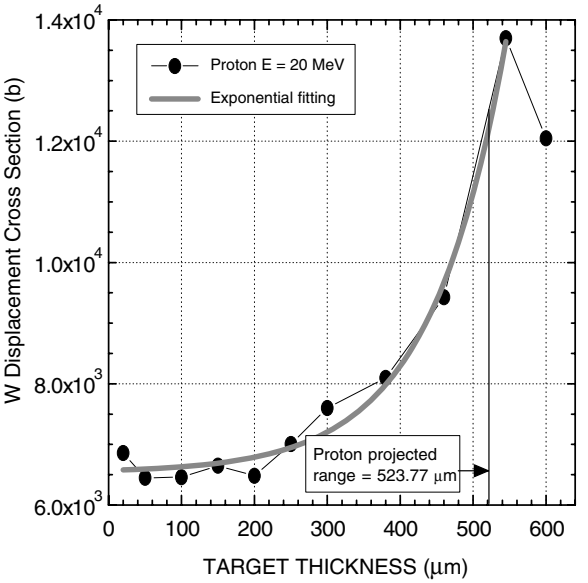

Fig. 4. Displacement cross section versus target thickness for 20 MeV protons on W from SRIM.

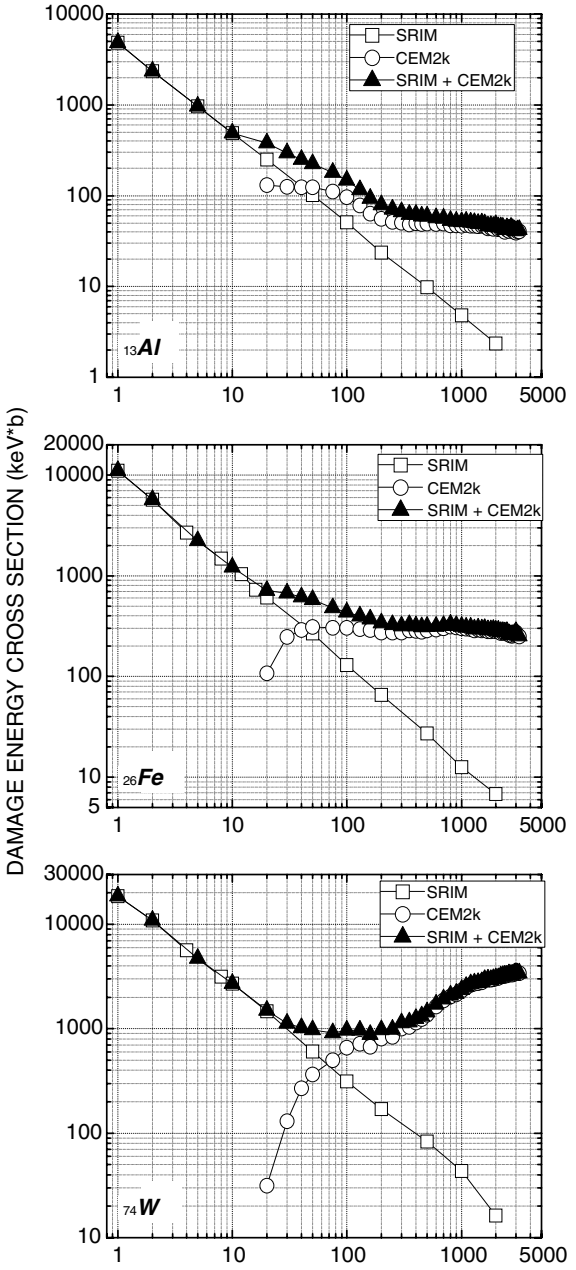

Fig. 5. Damage energy versus proton energy from SRIM, CEM2k, and SRIM+CEM2k.

approach may be to add the two types of cross sections. This is shown in Fig. 5 for Al, Fe, and W.

4. Displacement production due to protons at SINQ

It is interesting to see how such derived cross sections in Fig. 5 affect the calculation of proton-induced displacement production in a spallation neutron source. For this purpose the cross sections are folded accordingly into recently calculated proton fluxes at SINQ Target 5. Fig. 6 shows the diagram of Target 5 in STIP III (SINQ Target Irradiation Program III). The target vessel is double-wall-constructed containing mainly two types of rods. Rods shown to be 90% filled in Fig. 6 contain the Pb spallation target material. Those numbered are the rods containing specimens for spallation irradiation tests. Detailed description of Target 5 can be found in [14]. The calculation in [14] is recently revised due to a change of synthetic proton beam profile (truncated Gaussian distribution) to a gamma-scanned and more realistic beam profile. The assumed proton exposure of 10 Ahr is corrected to the practical exposure of 10.85 Ahr as well. The lowest tip of the Al entrance window and the centers containing Fe specimens at Rods 1 and 15 are examined as they stand, respectively, in the closest, middle and farthest position of the proton beam path. The investigation is to reveal how relatively the low energy displacement production (calculated by SRIM) and the high energy counterpart (calculated by INC's, i.e., CEM2k in our case) contribute to the total proton-induced displacement production. Fig. 7 shows the proton flux at the center of Rod 1 and the cumulative displacement production due

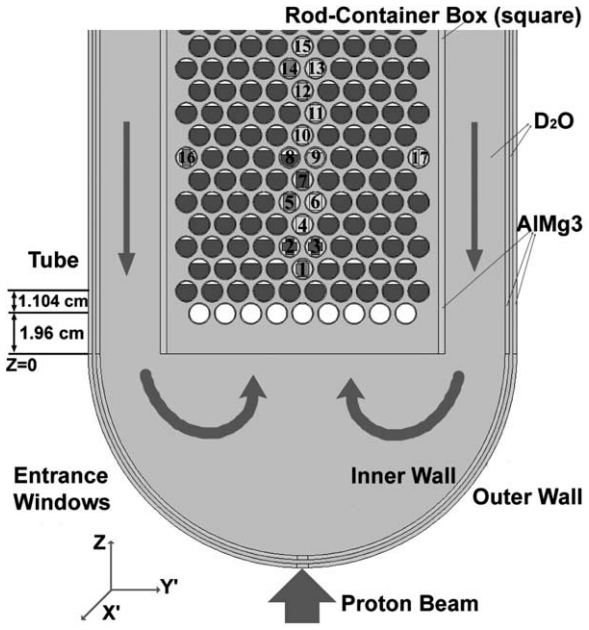

Fig. 6. Diagram of STIP III Target 5. Rods labeled with numbers 1–17 are specimen rods. Rods shown 90% filled are Pb target rods. The bottom layer contains empty rods.

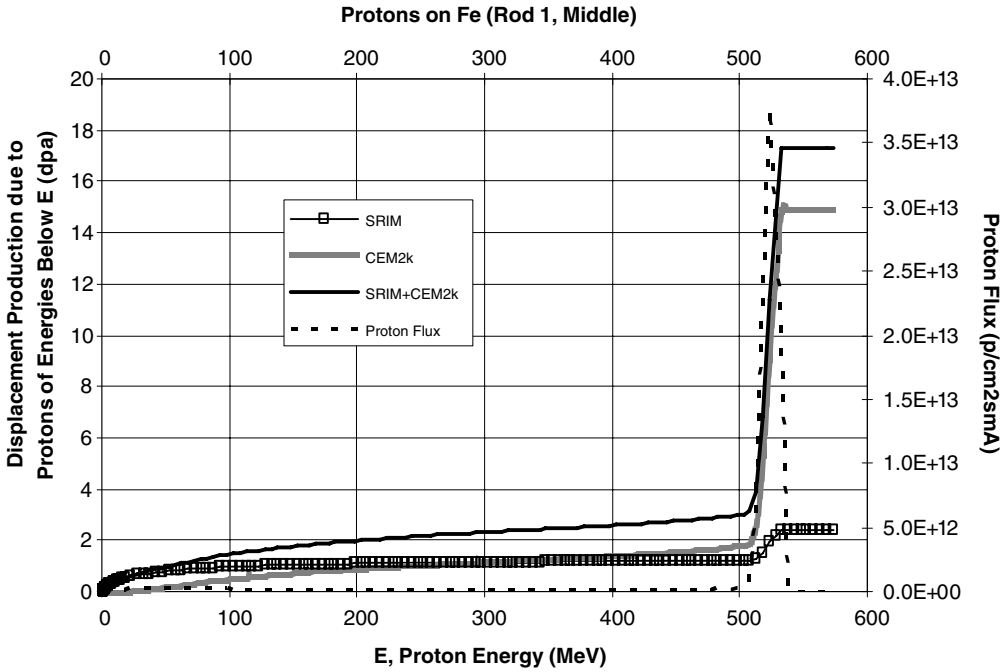

Fig. 7. Cumulative displacement production in Fe due to protons of energies below E at the center of Rod 1 in Target 5 STIP III. The calculation was done by folding the proton flux into the cross sections, respectively, from SRIM, CEM2k and their sum. The total exposure is 10.85 Ahr.

Table 1
Displacement concentration at the Al entrance window and in Fe at Rods 1 and 15 of SINQ Target 5 using SRIM, CEM2k, and their sum for an exposure of 10.85 Ahr

	Displacement concentration (dpa)		
	Al, window (%)	Fe, Rod 1 (%)	Fe, Rod 15 (%)
SRIM	1.1 (20)	2.4 (14)	2.0 (16)
CEM2k	4.3 (80)	14.9 (86)	10.2 (84)
Total	5.4 (100)	17.3 (100)	12.2 (100)

to proton energies below E by SRIM, CEM2k and the sum of them. As indicated in Table 1, the fractional displacement production due to SRIM can be as high as 14–20%, which is not negligible.

5. Benchmarking and recombination of radiation-produced defects

Remarks may be in order concerning the inherent difficulty in benchmarking calculated displacement cross sections, i.e., checking the validity of the calculated values on the basis of experimental observations. Resistivity annealing experiments on low-temperature-irradiated metals demonstrate that the radiation-produced increase in resistivity begins to anneal out at temperatures perhaps as low as 10 K (see, for example, [12], Chapter 6) due to thermally activated annihilation and clustering of point defects. There is also the possibility of spontaneous athermal motion and recombination of the point defects induced by atomic agitation within the original collision cascade. This idea is sometimes discussed in terms of a 'thermal spike,' i.e., a small volume of abnormal atomic motion within the cascade in which vacancies and interstitials recombine and displacements are annihilated. These factors would cause the calculated displacement cross section to be greater than the cross section deduced experimentally after some displacements were removed due to athermal spontaneous recombination or low-temperature thermally-activated annealing.

In the experimental study of Greene et al. [15], Cu and W resistivity samples were irradiated by 1.10- and 1.94-GeV protons at 4.7 K. Based on measurements of the radiation-produced increase in resistivity, experimental displacement cross sections were determined as shown by E(b) in Table 2. The corresponding values from our calculated displacement cross sections by Bertini and CEM2k are shown by C(b) in Table 2. We see that the

Table 2
Calculated (C) and experimental (E) displacement cross sections and $\eta = E/C$ values for protons on Cu and W. E cross sections by Greene et al. [14] using $\rho F = 2.0$ and 14.0 μohm-cm/at.% displacements for Cu and W, respectively. Threshold displacement energies: 40 eV for Cu and 90 eV for W

	E(b)	C(b) Bertini	$\eta = E/C$ **Bertini**	C(b) CEM2k	$\eta = E/C$ **CEM2k**
Cu, 1.1 GeV	1440	3380	**0.43**	4180	**0.34**
Cu, 1.94 GeV	1830	3080	**0.59**	3750	**0.49**
W, 1.1 GeV	4715	8080	**0.58**	11 110	**0.42**
W, 1.94 GeV	7895	8890	**0.89**	13 330	**0.59**

experimental-to-calculated ratio, $\eta = E/C$, ranges from about 0.3 to 0.9. Low values for these experimental-to-calculated ratios for displacement cross sections have also been reported for reactor neutron irradiation at 4.6 K [16] and for ion irradiation at 6 K [17].

The above discussion directs attention to the point of view that displacement rates based on calculated cross sections should be regarded as maximum rates, strictly true only under ideal conditions in which there is no athermal spontaneous defect recombination or low-temperature thermally-activated defect annealing.

References

[1] L.S. Waters, MCNPX User's Manual, Version 2.3.0, Report LA-UR-02-2607, Los Alamos National Laboratory, Los Alamos, New Mexico, 2002.
[2] S.G. Mashnik, A.J. Sierk, O. Bersillon, T. Gabriel, Nucl. Instr. Meth. A 414, 68, 1998. Also, Report LA-UR-97-2905, Los Alamos National Laboratory, Los Alamos, NM, 1997.
[3] V. McLane (Ed.), 'ENDF-102, Data Formats and Procedures for the Evaluated Nuclear Data File ENDF-6,' BNL-NCS-44945-01/04-Rev., National Nuclear Data Center, Brookhaven National Laboratory, Upton, New York, 2001.
[4] L.R. Greenwood and R.K. Smither, 'SPECTER: Neutron Damage Calculations for Materials Irradiations,' ANL/FPP/TM-197, Argonne National Laboratory, Argonne, Illinois, 60439, 1985.
[5] J.F. Ziegler, J.P. Biersack, U. Littmark, The Stopping and Range of Ions in Solids, Pergamon, New York, 1985, See also, www.srim.org.
[6] M.B. Chadwick, P.G. Young, S. Chiba, S.C. Frankle, G.M. Hale, H.G. Hughes, A.J. Koning, R.C. Little, R.E. MacFarlane, R.E. Prael, L.S. Waters, Cross section evaluations to 150 MeV for accelerator-driven systems and implementation in MCNPX, Nucl. Sci. Eng. 131 (1999) 293, See also, LA-UR-98-1825, Los Alamos National Laboratory, 1998.
[7] J. Lindhard, M. Scharff, H.E. Schiott, Range concepts and heavy ion ranges, notes on atomic collisions, II. Kongelige Danske Videnskabernes Selskab, Matematisk-Fysiske Meddelelser 33 (1963) 14, Copenhagen.
[8] Standard practice for neutron radiation damage simulation by charged-particle irradiation, E 521-96, Annual Book of ASTM Standards, Vol. 12.02, American Society for Testing and Materials, Philadelphia, 1996, p. 1.
[9] R.E. Prael, D.G. Madland, The LAHET Code System with LAHET 2.8, LA-UR-00-2140, Los Alamos National Laboratory, Los Alamos, New Mexico, 2000.
[10] E.J. Pitcher, P.D. Ferguson, G.J. Russell, R.E. Prael, D.G. Madland, J.D. Court, L.L. Daemen, M.S. Wechsler, The Effect of the New Nucleon–Nucleus Elastic Scattering Data in LAHET Version 2.8 on Neutron Displacement Cross Section Calculations, Materials for Spallation Neutron Sources, The Minerals, Metals, and Materials Society (TMS), Warrendale, PA, 1998.
[11] W. Lu, M.S. Wechsler, P.D. Ferguson, E.J. Pitcher, Spallation radiation damage calculations and database; cross-section discrepancies between the codes, J. ASTM Int. 3 (7) (2006). Available from: <www.astm.org.>.
[12] M.W. Thompson, Defects and Radiation Damage in Metals, Cambridge University, London, 1969.
[13] M.J. Norgett, M.T. Robinson, I.M. Torrens, Nucl. Eng. Des. 33 (1975) 50.
[14] W. Lu, M.S. Wechsler, Y. Dai, Calculations of radiation damage at SINQ Target 5, in: Proceedings, Sixth International Meeting on Nuclear Applications of Accelerator Technology (AccApp'03), American Nuclear Society, La Grange Park, Illinois, 2004, p. 438.
[15] G.A. Greene, C.L. Snead Jr., C.C. Finfrock, A.L. Hanson, M.R. James, W.F. Sommer, E.J. Pitcher, L.S. Waters, Direct measurements of displacement cross sections in copper and tungsten under irradiation by 1.1-GeV and 1.94-GeV Protons at 4.7 K, in: Proceedings, Sixth International Meeting on Nuclear Applications of Accelerator Technology (AccApp'03), American Nuclear Society, La Grange Park, Illinois, 2004, p. 881.
[16] G. Wallner, M.S. Anand, L.R. Greenwood, M.A. Kirk, W. Mansel, W. Waschkowski, J. Nucl. Mater. 152 (1988) 146.
[17] R.S. Averback, R. Benedeck, K.L. Merkle, Phys. Rev. B 18 (1978) 4156.